AFRL-RX-WP-JA-2017-0348

THIN-FILM MAGNETLESS FARADAY ROTATORS FOR COMPACT HETEROGENEOUS INTEGRATED OPTICAL ISOLATORS (POSTPRINT)

Dolendra Karki and Miguel Levy

Michigan Technological University

Vincent Stenger and Andrea Pollick

SRICO

27 April 2017
Interim Report

(STINFO COPY)

AIR FORCE RESEARCH LABORATORY
MATERIALS AND MANUFACTURING DIRECTORATE
WRIGHT-PATTERSON AIR FORCE BASE, OH 45433-7750
AIR FORCE MATERIEL COMMAND
UNITED STATES AIR FORCE

REPORT DOCUMENTATION PAGE

The public reporting burden for this collection of information is estimated to average 1 hour per response, including the time for reviewing instructions, searching existing data sources, gathering and maintaining the data needed, and completing and reviewing the collection of information. Send comments regarding this burden estimate or any other aspect of this collection of information, including suggestions for reducing this burden, to Department of Defense, Washington Headquarters Services, Directorate for Information Operations and Reports (0704-0188), 1215 Jefferson Davis Highway, Suite 1204, Arlington, VA 22202-4302. Respondents should be aware that notwithstanding any other provision of law, no person shall be subject to any penalty for failing to comply with a collection of information if it does not display a currently valid OMB control number. **PLEASE DO NOT RETURN YOUR FORM TO THE ABOVE ADDRESS.**

1. REPORT DATE *(DD-MM-YY)*	2. REPORT TYPE	3. DATES COVERED *(From - To)*
27 April 2017	Interim	9 May 2016 – 1 December 2016

4. TITLE AND SUBTITLE
THIN-FILM MAGNETLESS FARADAY ROTATORS FOR COMPACT HETEROGENEOUS INTEGRATED OPTICAL ISOLATORS (POSTPRINT)

5a. CONTRACT NUMBER
FA8650-16-M-5026

5b. GRANT NUMBER

5c. PROGRAM ELEMENT NUMBER
65502F

6. AUTHOR(S)
1) Dolendra Karki and Miguel Levy – Michigan Technological University
2) Vincent Stenger and Andrea Pollick – SRICO

5d. PROJECT NUMBER
3005

5e. TASK NUMBER

5f. WORK UNIT NUMBER
X16Q

7. PERFORMING ORGANIZATION NAME(S) AND ADDRESS(ES)
1) Michigan Technological University
1400 Townsend Drive
Houghton, MI 49931

2) SRICO, Inc.
2724 Sawbury Blvd.
Columbus, OH 43235

8. PERFORMING ORGANIZATION REPORT NUMBER

9. SPONSORING/MONITORING AGENCY NAME(S) AND ADDRESS(ES)
Air Force Research Laboratory
Materials and Manufacturing Directorate
Wright-Patterson Air Force Base, OH 45433-7750
Air Force Materiel Command
United States Air Force

10. SPONSORING/MONITORING AGENCY ACRONYM(S)
AFRL/RXAN

11. SPONSORING/MONITORING AGENCY REPORT NUMBER(S)
AFRL-RX-WP-JA-2017-0348

12. DISTRIBUTION/AVAILABILITY STATEMENT
Distribution Statement A. Approved for public release: distribution unlimited.

13. SUPPLEMENTARY NOTES
PA Case Number: 88ABW-2017-2013; Clearance Date: 27 Apr 2017. This document contains color. Journal article published in Journal of Applied Physic, Vol. 121, No. 23, 21 Jun 2017. © 2017 AIP Publishing. The U.S. Government is joint author of the work and has the right to use, modify, reproduce, release, perform, display, or disclose the work. The final publication is available at http://dx.doi.org/10.1063/1.4986237

14. ABSTRACT *(Maximum 200 words)*

This report describes the fabrication, characterization, and transfer of ultra-compact thin-film magnetless Faraday rotators to silicon photonic substrates. Thin films of magnetization latching bismuth-substituted rare-earth iron garnets were produced from commercially available materials by mechanical lapping, dice polishing, and crystal-ion-slicing. Eleven-μm-thick films were shown to retain the 45Faraday rotation of the bulk material to within 2at 1.55 μm wavelength without repoling. Anti-reflection coated films evince 0:09 dB insertion loses and better than –20 dB extinction ratios. Lower extinction ratios than the bulk are ascribed to multimode propagation. Significantly larger extinction ratios are predicted for single-mode waveguides. Faraday rotation, extinction ratios, and insertion loss tests on He-ion implanted slab waveguides of the same material yielded similar results. The work culminated with bond alignment and transfer of 7 μm -thick crystal-ion-sliced 50 x 480 μm 2 films onto silicon photonic substrates.

15. SUBJECT TERMS
Faraday effect . Wave attenuation . Planar waveguides . Garnet . Photonics

16. SECURITY CLASSIFICATION OF:

a. REPORT	b. ABSTRACT	c. THIS PAGE
Unclassified	Unclassified	Unclassified

17. LIMITATION OF ABSTRACT:
SAR

18. NUMBER OF PAGES
8

19a. NAME OF RESPONSIBLE PERSON (Monitor)
Robert Nelson

19b. TELEPHONE NUMBER *(Include Area Code)*
(937) 255-9907

Thin-film magnetless Faraday rotators for compact heterogeneous integrated optical isolators

Dolendra Karki,[1] Vincent Stenger,[2] Andrea Pollick,[2] and Miguel Levy[1]

[1]*Physics Department, Michigan Technological University, Houghton, Michigan 49931, USA*
[2]*SRICO, Inc., Columbus, Ohio 43235, USA*

This report describes the fabrication, characterization, and transfer of ultra-compact thin-film magnetless Faraday rotators to silicon photonic substrates. Thin films of magnetization latching bismuth-substituted rare-earth iron garnets were produced from commercially available materials by mechanical lapping, dice polishing, and crystal-ion-slicing. Eleven-μm-thick films were shown to retain the 45° Faraday rotation of the bulk material to within 2° at 1.55 μm wavelength without re-poling. Anti-reflection coated films evince 0.09 dB insertion loses and better than –20 dB extinction ratios. Lower extinction ratios than the bulk are ascribed to multimode propagation. Significantly larger extinction ratios are predicted for single-mode waveguides. Faraday rotation, extinction ratios, and insertion loss tests on He-ion implanted slab waveguides of the same material yielded similar results. The work culminated with bond alignment and transfer of 7 μm-thick crystal-ion-sliced $50 \times 480 \, \mu$m^2 films onto silicon photonic substrates. *Published by AIP Publishing.*
[http://dx.doi.org/10.1063/1.4986237]

I. INTRODUCTION

The miniaturization of optical isolators and circulators has been actively pursued over the last several decades.[1–3] This effort has been spurred by a widespread industrial need, particularly in optical telecommunications, to protect laser sources from return light and back reflections in optical circuits.[1–3] Driving factors for this undertaking include the expected robustness of integrated circuits, improved functional reliability, batch fabrication economy, improved optical alignment, and immunity to vibrations.

Magneto-optic methodologies to on-chip isolation have received considerable attention because of the nonreciprocal nature of the Faraday Effect and the magneto-optic nonreciprocal phase-shift effect.[1–3] Both these techniques require the application of a magnetic field to saturate the magnetization in the device. Magneto-optic garnet materials, most notably bismuth- and cerium-substituted iron garnets, have been used in on-chip prototypes. These are also the materials of choice and are extensively used in bulk isolators sold commercially at present.

Most of the work devoted to the development of compact on-chip isolators has focused on the design and fabrication of optical waveguide structures, such as Faraday rotators,[4–6] Mach-Zehnder interferometers,[7–9] ring resonators,[10,11] and other variants.[12–14] But the remaining issue of reducing the size or eliminating the magnetizing element, be it permanent magnets or electromagnets, has not been addressed extensively.[6,15,16] In fact, it is the magnetizing element which accounts for a considerable part of the bulk of these devices at present. Prior work by one of the co-authors has addressed the integration of permanent magnet films in Faraday rotator waveguide structures.[6,15] But no work has been reported on the complete elimination of the magnetizing element in micron-scale magneto-optic devices. It is this question that is addressed here.

In addition, this article also addresses the critical figures of merit in optical isolation, besides the elimination of magnet bulk, namely, insertion loss and isolation ratio. Isolation ratios compare the forward optical power transmitted by the device to the backward propagating light reaching the laser source. The results presented here show the lowest insertion losses achieved so far for miniaturized Faraday rotators, comparable to those in bulk isolators sold commercially, and are comparable to the best isolation ratios achieved with on-chip devices.[1–3] This superior performance stems from the high quality of the liquid-phase-epitaxially grown (LPE) materials used in our work and the processing techniques reported here. Of particular note is our use of crystal-ion-slicing, an ion-implantation-based technique to detach and transfer micron-scale-thick film samples from high-quality bulk materials that sidesteps the need for lattice-matched epitaxial growth on the optical platform.[17,18]

Liquid-phase-epitaxially grown bismuth-substituted iron garnet mono-crystal materials are regularly used in technologically important nonreciprocal photonic components, including optical isolators, circulators, and switches. These materials are especially valued for their high-optical quality, particularly low-loss and large Faraday rotations in the infrared telecom wavelength range.

Latching Faraday-rotator LPE iron-garnets have the additional remarkable attribute that they do not require bias magnets for their operation. This significant feature makes it possible to greatly reduce rotator device size relative to designs that require an external applied magnetic field. At 1.55 μm-wavelength, they typically display 0.43 dB/cm optical absorption and 938 deg/cm (1745 rad/m) Faraday rotation, making them ideal nonreciprocal device materials.

The key to magnetless operation resides in the composition of the garnet. A saturated magnetic state without bias magnets is achieved through maximizing the incorporation of

europium (Eu) in order to reduce the saturation magnetization of the garnet without creating a compensation point.[19,20] The nominal composition of the garnet is Bi_X $(Eu_Z Ho_{1-Z})_{3-X}$ $Fe_{5-Y} Ga_Y O_{12}$ per formula unit.

These materials are grown on (111)-oriented single-crystal Ca/Mg/Zr-substituted gadolinium gallium garnet (CMZ-GGG) substrates, and their integration into silicon or into other non-compatible platforms has not been demonstrated. As grown, their magnetization axis is normal to the plane of the film (Fig. 1(a)). Therefore, the on-chip integration of these Faraday rotators into alternative platforms requires post-LPE-growth manufacturing to form a new thin-film-plane. Its normal should be perpendicular to the growth direction, as shown in Fig. 1(b). The optical propagation axis must be along the magnetization direction.

This letter reports on the fabrication of such films and their integration into silicon-on-insulator (SOI) and other platforms. It is shown that processed films via mechanical thin-down lapping retain their magnet-less latching character and their original bulk Faraday rotations without re-poling to within experimental error. Film-transfer onto silicon photonic chips by crystal-ion-slicing is also described. This latter technique was originally introduced by one of the co-authors several years ago for non-latching iron garnets and is here extended to latching materials.[17] Tests show that ion-implanted samples exhibit minimal changes in magneto-optical properties from the bulk and excellent optical transmission, as detailed below.

II. PROCESSING AND MAGNETO-OPTICAL PROPERTIES OF MECHANICALLY PROCESSES THIN-FILMS

Anti-reflection-coated 480 μm-thick, 10×10 mm^2 latching Faraday-rotator pieces were procured from Integrated Photonics, Inc. These materials retain their magnetization without externally applied magnetic fields for their operation. The pieces were cut to produce 45° rotations at normal incidence. Faraday rotation and insertion loss measurements on the as-procured samples at 1.55 μm wavelength performed in our laboratory yielded 44.3°±1.3° and 0.02 dB, respectively.

Strips measuring 2 mm × 10 mm × 480 μm were cut off from the original pieces, with the magnetization direction along the 480 μm-long side. The 2 mm × 10 mm facets remained anti-reflection-coated on both sides. These strips were crystal-wax-bonded to silicon platforms and the 2 mm side was thinned down via diamond-film lapping. The finest diamond particle size used for polishing was 0.25 μm. Films of three different thicknesses 11 μm, 50 μm, and 300 μm were produced. Figure 2 shows scanning-electron-micrographs (SEM) of the first two types.

Figure 3 depicts the Faraday rotation testing setup used to characterize the processed films. A lensed fiber couples linearly polarized light into the Faraday rotator. The light is vertically confined in the film but diffracts laterally, as evidenced by the output image (Fig. 3, inset) from the 11 μm-thick sample. A Glan-Thomson polarizer allows us to analyze the angular-dependence of the output polarization.

Faraday rotations, insertion losses, and extinction ratios for the three mechanically polished films, all without re-poling, are shown in Table I. Extinction ratios are defined as the power ratios between minimum and maximum transmission powers for the Faraday rotations, in dB. For the purposes of this table, we define Faraday rotation as the direction of the semi-major axis of the rotated polarization ellipse. The rotations are exhibited for opposite propagation directions, where forward propagation is defined in the magnetization direction. Uncertainties correspond to one standard deviation from average values taken over several measurements in each case. Also displayed in the table is the response for the bulk material. The polarization response of the 11 μm-thick film as a function of analyzer angle for one of these measurements is shown in Fig. 4.

III. MODE BIREFRINGENCE AND FARADAY ROTATION

Slab waveguides introduce a disparity between transverse-electric (TE) and transverse magnetic (TM) mode indices (linear birefringence) in addition to the existing circular birefringence inherent in the Faraday effect. As a consequence, the output polarization acquires some degree of ellipticity and suffers rotational departures from that of the bulk material. However, it was found that this effect is
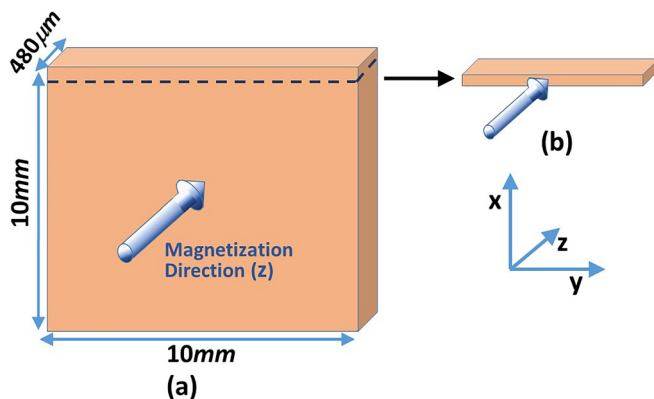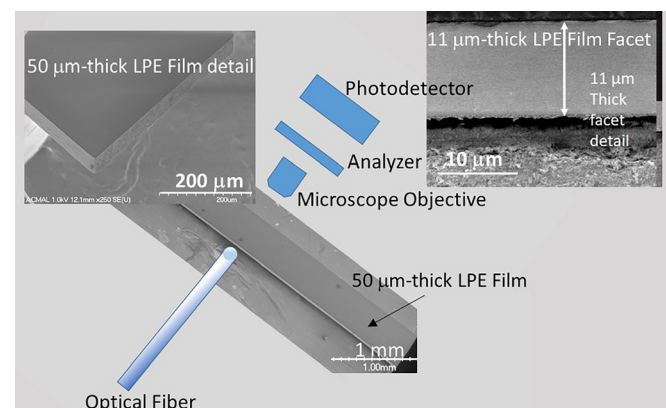

FIG. 1. Geometry of the latching Faraday rotators. The magnetization direction is normal to the large faces. (Drawing not to scale.)

FIG. 2. 50 μm-thick film cross-sectional SEM images, with schematic depiction of the optical fiber and detection components used for Faraday rotation testing. 11 μm-thick film facet cross-sectional SEM image.
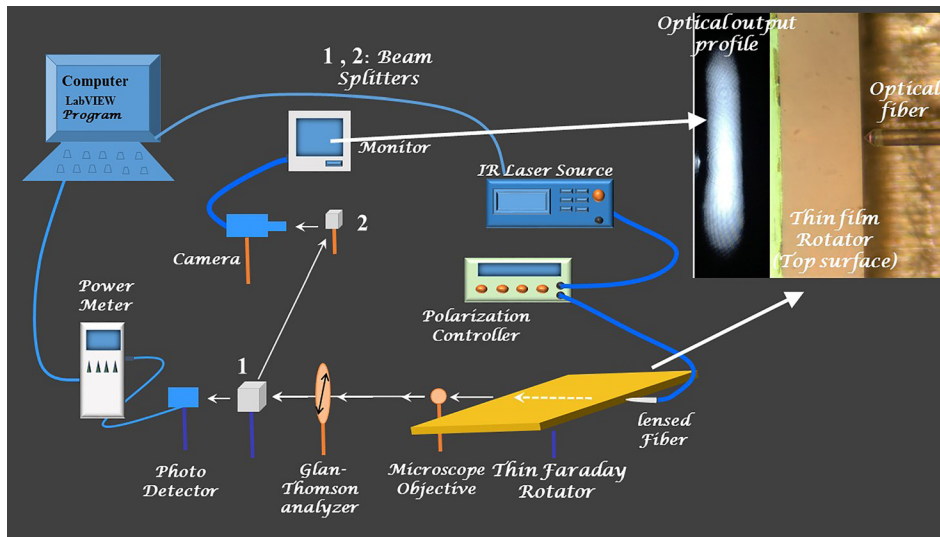
FIG. 3. Testing set-up for measuring Faraday rotation in the latching iron garnet film samples. The inset shows the diffracted output image from the 11 μm-thick film. It also shows a top view of the lensed fiber tip and the top surface of the film.

negligible for 300 μm- and 50 μm-thick films and relatively small for 11 μm-thick films.

In the presence of linear birefringence, the otherwise circularly polarized counter-gyrating normal modes of the Faraday rotator become elliptically polarized. And their phase difference after any given propagation length L changes as well. Given an intrinsic Faraday rotation angle per unit length θ_F and linear birefringence between TE and TM modes $n_{TE} - n_{TM}$, the phase mismatch between counter-gyrating elliptical normal modes after a distance L becomes

$$\phi = 2L\sqrt{\theta_F^2 + \left[\frac{\pi}{\lambda}(n_{TE} - n_{TM})\right]^2}, \qquad (1)$$

where λ is the free-space wavelength.

Taking into account the calculated geometrical birefringence $n_{TE} - n_{TM}$ for an 11 μm-thick iron-garnet slab with crystal bond, bottom cladding yields the following polarization rotations and extinction ratios for the first four waveguide modes (Table II). These are obtained making use of the calculated phase mismatch from Eq. (1). We assume $\theta_F L = 45°$, film index = 2.35, bottom cladding index = 1.5277, and $\lambda = 1.55$ μm.

Notice that the observed 11 μm-thick film extinction ratio displayed in Table I is consistent with the detrimental presence of higher-order modes in the slab waveguide. Other effects such as film-surface roughness and stress birefringence cannot be completely ruled out. A single-mode structure, achievable through additional processing (thinning and patterning) should, theoretically, yield extinction ratios higher than –30 dB, as predicted in Table II.

IV. POLARIZATION ROTATION TESTS ON SLAB WAVEGUIDES FORMED BY ION IMPLANTATION

Crystal ion slicing proceeds via energetic He-ion implantation into metal oxides.[17,18] In this work, the ions were accelerated to an energy of 3.5 MeV and deposited at a dose of 5×10^{16} cm^{-2}. Rapid thermal annealing (RTA) under nitrogen flow for 30 s in the temperature range of 700 °C to 800 °C produced best results.

A low-refractive-index sacrificial layer due to the implantation forms below the surface that is then etched away to detach the top film from the rest of the sample. This sacrificial layer can act as a cladding layer for slab waveguiding prior to detachment.

The Faraday rotation and insertion loss of linearly polarized light passing through these slab waveguides were characterized for different post-implantation rapid-thermal-annealing (RTA) preparation conditions. It was found that the magneto-optic response depended on RTA, approaching bulk material response at higher tested annealing temperatures. The output intensity profile after propagation is shown in the inset in Fig. 5. Butt coupling from the lensed fiber
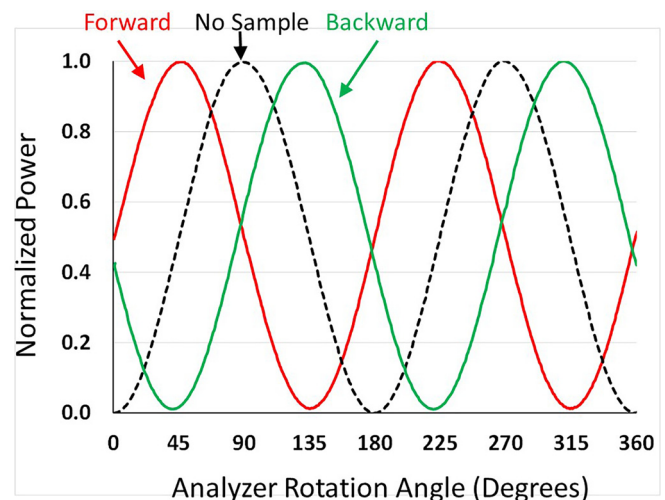
TABLE I. Faraday rotations, extinction ratios, and insertion losses for mechanically polished films without re-poling.

Sample	Forward FR	Backward FR	Extinction	Insertion loss
Bulk	44.7°±0.9°	44.5°±0.6°	<−30 dB	0.02 dB
300 μm-thick	45.2°±1.0°	44.3°±0.9°	<−30 dB	NA
50 μm-thick	45.6°±0.8°	44.2°±0.5°	<−30 dB	NA
11 μm-thick	46.7°±2.1°	41.9°±1.9°	−20.5±2.0 dB	0.09±0.01 dB

FIG. 4. 360° analyzer rotation scans with and without 11 μm-thick sample in the beam path.

TABLE II. Calculated polarization rotations and extinction ratios for the first four waveguide modes of an 11 μm-thick iron-garnet slab at $\lambda = 1.55 \mu$m.

Waveguide mode	$n_{TE} - n_{TM}$	Polarization rotation	Extinction ratio
Fundamental	0.000025	45.17°	−34.0 dB
First	0.000103	45.30°	−23.7 dB
Second	0.000231	45.50°	−15.9 dB
Third	0.000414	45.90°	−11.7 dB
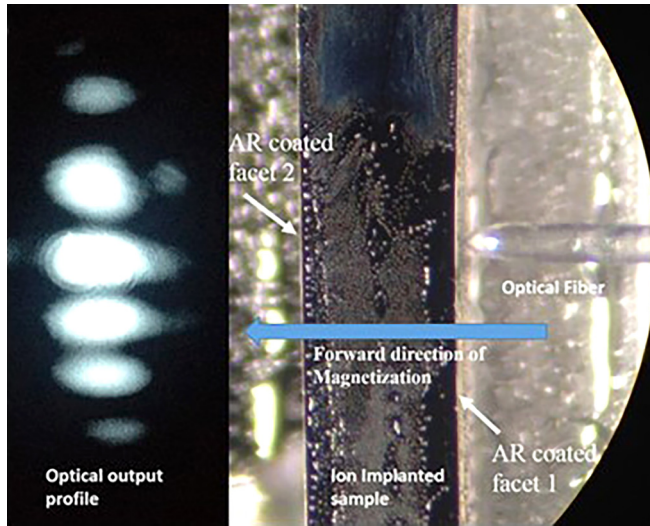
FIG. 5. Fiber launch configuration and mode profile for the ion implanted sample.

FIG. 6. 360° polarizer rotation scans with and without the sample in the beam path (no external magnetizing field). Data at 1.55 μm wavelength.
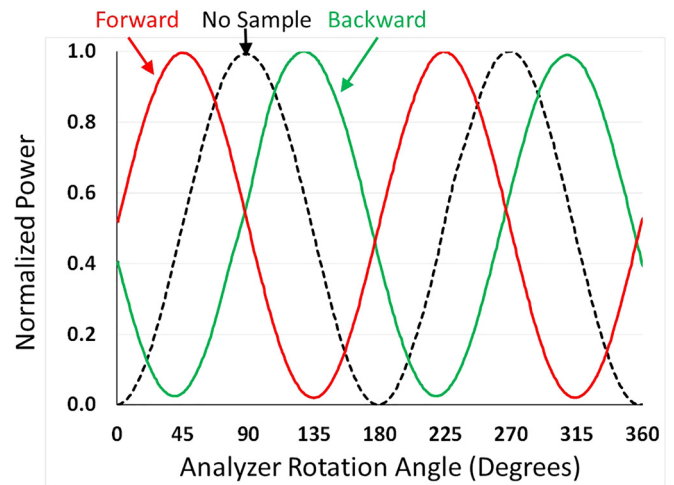
onto the anti-reflection (AR) coated facet of the slab waveguide is also shown.

A comparison of the magneto-optical response in the ion-implanted slab waveguides with mechanically thinned-down films evinces a more pronounced polarization ellipticity and somewhat larger departures from bulk Faraday rotation in the former. These more pronounced departures from bulk behavior in the ion-implanted slabs are consistent with a smaller waveguide thickness and the presence of high-order waveguide modes. Table III compares the performance in these two types of waveguides. The polarization ellipticity amelioration at higher RTA temperatures, referred to before, is also consistent with implantation-damage repair and segregation of residual crystal defects away from the waveguide core and towards the sacrificial layer. Figure 6 shows 360° analyzer rotation scans with and without the ion-implanted sample in the beam path, without re-poling.

Table IV exhibits the calculated departures from intrinsic Faraday rotation and power extinction ratios in 8 μm-thick slab waveguides as a result of mode birefringence. These results are consistent with the more pronounced departures

as compared with the 11 μm-thick film. Insertion loss data in the ion-implanted slab waveguide were also measured at 1.55 μm wavelength and found to be 0.12±0.01 dB, slightly higher than the 0.09±0.01 dB in the unimplanted sample (Table III). We tentatively ascribe this higher optical loss to residual post-anneal implantation-induced lattice damage in the core and cladding lattice defects in the optical waveguide.

V. CRYSTAL-ION SLICING OF MAGNETLESS THIN-FILM FARADAY ROTATORS

Crystal-ion-slicing involves the ion implantation of energetic light ions to generate a sacrificial damage layer below the sample surface.[17,18] This induces differential etching that undercuts the top layer when the sample is immersed in phosphoric acid to release the film. Rapid thermal annealing prior to etching repairs residual damage due to the ion trajectories above the sacrificial layer and enhances the differential etch rate with the sacrificial layer.

Prior work has shown crystal ion-sliced transfer of magnetic garnet films onto GaAs platforms.[17] Here, a similar process was used to demonstrate the transfer of bias-free latching iron garnet films onto temporary handle substrates and characterize their Faraday rotation and insertion losses after ion-implantation prior to slicing. Future work will characterize their magneto-optic properties after full transfer.

TABLE III. Comparison of the magneto-optical response of ion-implanted slab waveguides with mechanically thinned-down films.

Waveguide	Forward FR	Backward FR	Extinction	Insertion loss
11 μm	46.7°±2.1°	41.9°±1.9°	−20.5±2.0 dB	0.09±0.01 dB
8 μm, Implanted	44°	40.7°	−17 dB	0.12±0.01 dB

TABLE IV. Calculated slab waveguide mode polarization-rotation departures from 45° (semi-major axis of polarization ellipse) in Faraday rotator due to mode birefringence. Slab and substrate refractive indices are assumed to be 2.35 and 1.95, respectively. Slab thickness is 8 μm.

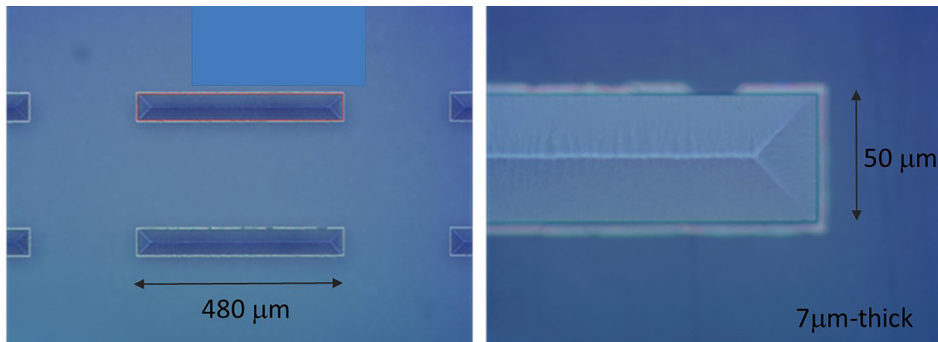| Waveguide mode	Departure from 45°	Power extinction ratio
Fundamental	±0.4°	−28.5 dB
First	±0.5°	−15.9 dB
Second	±3.4°	−9.5 dB
Third	±10.4°	−4.6 dB

FIG. 7. Magnetless iron garnet films on temporary handle substrate after ion slicing. Detail on the right panel.
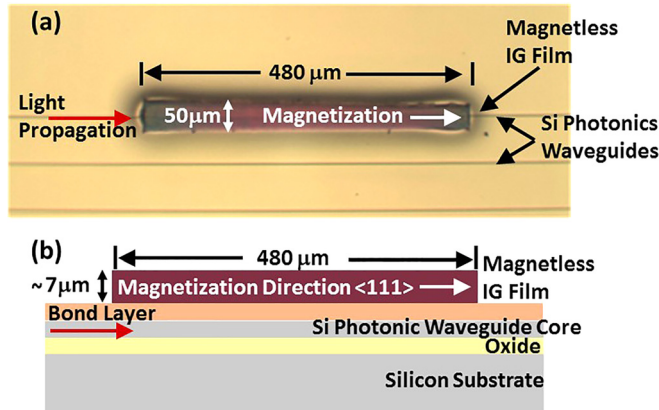

FIG. 8. Magnetless iron garnet (IG) film bond-align transferred to a silicon photonic substrate. (a) Top microscope image of bond-aligned film and (b) side view illustration showing the various material layers.

Latching Faraday rotator samples were prepared for ion implantation to produce in-plane magnetized crystal-ion-sliced films, with magnetization axis along the propagation direction, as shown in Fig. 1. The as-received $10 \, mm \times 10 \, mm \times 480 \, \mu m$ samples were cut into strips $10 \, mm \times 1 \, mm \times 480 \, \mu m$ using a precision dice polishing process. The strips were then mounted for implantation normal to the $10 \, mm \times 480 \, \mu m$ face in order to form optical slab waveguides for Faraday rotation and absorption loss measurements prior to wet-etch and release of the films.

After implant, additional dice polish trenching of the implanted surface was done to form $50 \, \mu m$ wide rectangular features of various lengths from $100 \, \mu m$ to $480 \, \mu m$. After bonding to a temporary handle wafer, crystal-ion slicing was done by wet etching to transfer the iron garnet films to the handle wafer. Figure 7 shows arrays of transferred films on a temporary handle wafer.

VI. TRANSFER TO Si PHOTONIC SUBSTRATES

Temporary mounted sliced magnetless iron garnet films of $7 \, \mu m$ thickness were bond-aligned and transferred to silicon photonic substrate by permanent adhesive bonding. An example of a bond aligned film is shown in Fig. 8. The film may be made to vertically couple to the underlying silicon waveguide by evanescent, reverse taper, grating, or other coupling methods. Alternatively, the film may be aligned and placed in a pre-milled slot in the silicon photonic substrate.

VII. CONCLUSIONS

In this work, fabrication, characterization, and transfer of thin-film magnetless Faraday rotators to silicon photonic substrates have been demonstrated. Faraday rotations remain within $2°$ of bulk performance in $45°$ rotators, with extinction ratios better than $-20 \, dB$ and insertion losses lower at $0.09 \, dB$ for $11 \, \mu m$-thick films. Departures from better than $-30 \, dB$ bulk performance are ascribed mainly to the presence of high-order waveguide modes in the films and can be eliminated via single-mode structures. The magnetless film processing methodology developed in this work may be used to produce compact and high performance heterogeneous integrated isolators and circulators in silicon photonic substrates or in other semiconductor photonic platforms.

ACKNOWLEDGMENTS

[1] B. J. H. Stadler and T. Mizumoto, "Integrated magneto-optical materials and isolators: A review," IEEE Photonics J. **6**, 0600215 (2014).

[2] T. Mizumoto, R. Takei, and Y. Shoji, "Waveguide optical isolators for integrated optics," IEEE J. Quantum Electron. **48**, 252–260 (2012).

[3] M. Levy, "The on-chip integration of magnetooptic waveguide isolators," IEEE J. Sel. Top. Quantum Electron. **8**, 1300–1306 (2002).

[4] R. Wolfe, V. J. Fratello, and M. McGlashan-Powell, "Thin-film garnet materials with zero birefringence for magneto-optic waveguide devices," J. Appl. Phys. **63**, 3099–3103 (1988).

[5] R. Wolfe, R. A. Lieberman, V. J. Fratello, R. E. Scotti, and N. Kopylov, "Etch-tuned ridged waveguide magneto-optic isolator," Appl. Phys. Lett. **56**, 426–428 (1990).

[6] M. Levy, R. M. Osgood, Jr., H. Hegde, F. J. Cadieu, R. Wolfe, and V. J. Fratello, "Integrated optical isolators with sputter-deposited thin-film magnets," IEEE Photonics Technol. Lett. **8**, 903–905 (1996).

[7] J. Fujita, M. Levy, R. M. Osgood, Jr., L. Wilkens, and H. Dötsch, "Waveguide optical isolator based on Mach-Zehnder interferometer," Appl. Phys. Lett. **76**, 2158–2160 (2000).

[8] Y. Shoji, T. Mizumoto, H. Yokoi, I.-W. Hsieh, and R. M. Osgood, Jr., "Magneto-optical isolator with silicon waveguides fabricated by direct bonding," Appl. Phys. Lett. **92**, 071117 (2008).

[9] S. Ghosh, S. Keyvaninia, Y. Shoji, W. Van Roy, T. Mizumoto, G. Roelkens, and R. G. Baets, "Compact Mach–Zehnder interferometer Ce:YIG/SOI optical isolators," IEEE Photonics Technol. Lett. **24**, 1653–1656 (2012).

[10] M.-C. Tien, T. Mizumoto, P. Pintus, H. Kromer, and J. E. Bowers, "Silicon ring isolators with bonded nonreciprocal magneto-optic garnets," Opt. Express **19**, 11740–11745 (2011).

[11]L. Bi, J. Hu, P. Jiang, D. H. Kim, G. F. Dionne, L. C. Kimerling, and C. A. Ross, "On-chip optical isolation in monolithically integrated nonreciprocal optical resonators," Nat. Photonics **5**, 758–762 (2011).

[12]H. Dammann, E. Pross, G. Rabe, and W. Tolksdorf, "45° Waveguide isolators with phase mismatch," Appl. Phys. Lett. **56**, 1302–1304 (1990).

[13]J. M. Hammer, J. H. Abeles, and D. J. Channin, "Polycrystalline-metal-ferromagnetic optical waveguide isolator (POWI) for monolithic-integration with diode-laser devices," IEEE Photonics Technol. Lett. **9**, 631–633 (1997).

[14]T. Shintaku, "Integrated optical isolator based on efficient nonreciprocal radiation mode conversion," Appl. Phys. Lett. **73**, 1946–1948 (1998).

[15]M. Levy, I. Ilic, R. Scarmozzino, R. M. Osgood, Jr., R. Wolfe, C. J. Gutierrez, and G. Prinz, "Thin-film-magnet magnetooptic waveguide Isolator," IEEE Photonics Technol. Lett. **5**, 198–200 (1993).

[16]H. Lira, Z. Yu, S. Fan, and M. Lipson, "Electrically driven nonreciprocity induced by interband photonic transition on a silicon chip," Phys. Rev. Lett. **109**, 033901 (2012).

[17]M. Levy, R. M. Osgood, Jr., A. Kumar, and H. Bakhru, "Epitaxial liftoff of thin oxide layers: Yttrium iron garnets onto GaAs," Appl. Phys. Lett. **71**, 2617 (1997).

[18]M. Levy, R. M. Osgood, Jr., R. Liu, L. E. Cross, G. S. Cargill III, A. Kumar, and H. Bakhru, "Fabrication of single-crystal lithium niobate films by crystal ion slicing," Appl. Phys. Lett. **73**, 2293 (1998).

[19]C. D. Brandle, Jr., V. J. Fratello, and S. J. Licht, "Article comprising a magneto-optic material having low magnetic moment," U.S. patent 5,608,570 (March 4, 1997).

[20]R. R. Abbott, V. J. Fratello, S. J. Licht, and I. Mnushkina, "Article comprising a Faraday rotator that does not require a bias magnet," U.S. patent 6770223 B1 (August 3, 2004).